Nano World Journal

https://doi.org/10.17756/nwj.2023-s1-043

Research Article

Open Access

The Application of the TOPSIS Method to Identify the Optimal Machining Parameters during the Machining of the Mg-Ca Treated Nickel-Chromium (EN 36C) Case-hardened Steel

Vishal Mishra and Kalyan Chakraborty*

National Institute of Technology, Silchar, Assam, India

***Correspondence to:**
Kalyan Chakraborty
National Institute of Technology,
Silchar, Assam, India.
E-mail: kalyan.ch2013@gmail.com

Received: November 24, 2022
Accepted: April 12, 2023
Published: April 14, 2023

Citation: Mishra V, Chakraborty K. 2023. The Application of the TOPSIS Method to Identify the Optimal Machining Parameters during the Machining of the Mg-Ca Treated Nickel-Chromium (EN 36C) Case-hardened Steel. *NanoWorld J* 9(S1): S215-S219.

Published by United Scientific Group

Abstract

A Tungaloy coated carbide tool insert was used to machine the Calcium-Magnesium treated EN 36C steel. Speed (v), feed (f), and depth of cut (DOC) were the input parameters. The chip reduction coefficient (CRC) and the von Mises stress (VMS) were the machining responses. The L_{27} orthogonal array according to the Taguchi design plan was selected for the machining. The TOPSIS (Technique for Order of Preference by Similarity to Ideal Solution) method was applied to find out the optimal machining parameters. The optimal condition was identified as a speed of 100 m/min, a feed of 0.63 mm/rev, and a DOC of 0.67 mm. The scanning electron microscopy (SEM) and EDX (Energy-dispersive X-ray spectroscopy) analysis for the chips were done. The optimal solution can be validated by SEM and EDX studies for the chip and the tool. The machinability of the alloy was improved because of the built-up layer (BUL) formation during high-speed machining. All the machining parameters were found to interact with the machining responses. The attainment of the optimal solution is due to the influence of feed at high speed and low DOC.

Keywords

Coated carbide, von Mises stress, Machinability, Alloy

Introduction

The nickel (Ni) chromium (Cr) case hardened steel is extensively used for its superior mechanical properties. EN 36C steel is used to produce the crankshafts, connecting rods, shafts, gear wheels, and collets. The non-metallic inclusions improve the machinability of the alloy. The high strength free cutting steel was machined by using the AlSiTiN coated tool with reference to the machining forces, friction coefficient, etc. The improvement in the machinability of the material occurred due to the BUL formation for the higher speed [1]. The austenitic stainless steel (AISI 310) was machined for different speeds, feeds, and DOC. The cutting speed significantly influenced the BUE and BUL formations [2]. The Ca-treated steel was machined by using a CVD-coated cutting tool. The sulfide grains (round) and the aluminate grains (deformed elongated) were observed on the tool rake face. The BUL formation is based on the mechanical process for the influence of the compressive stress [3]. The austenitic-graded steel was machined to study the influence of microstructures on tool wear. The inclusion layer formed during the machining acts as the diffusion barrier and inhibits tool wear [4]. The Ca-treated carburizing steel was hard turned using the PCBN tool. The tool life for the Ca-treated steel was significantly higher. The machinability of the steel was significantly improved due to the (Mn, Ca) S and (Ca, Al) (O, S) inclusions [5]. The machinability of Ni-Cr case hardened steel can be improved by tempering the alloy [6]. The effects of the non-metallic inclusions in the PDZ were investigated. The influences of the composition, size, number,

and geometry of the inclusions on the tool wear and power consumption were investigated [7]. The prior austenite grain boundaries can be identified by carburizing the Ni-Cr low carbon steels. The mechanical properties of Ni-Cr low carbon steel are enhanced due to the Ni and Cr carbide [8]. The medium carbon Cr-Mo steel containing high sulfur content was Ca-treated. Machinability was found to be improving. The mechanical properties of the alloy were not affected by the higher sulfur content with reference to the steel for the low sulfur content [9]. The tool temperature during machining of the Ca-treated stainless steel (316L) with the high sulfur content was lower in comparison to the same steel with low sulfur content [10]. Efforts were made to modify the influence of MnS and Al_2O_3 inclusions by the Mg-Ca treatment in 16MnCrS5 and 49MnVS3 steels containing Ni-Mg alloy [11]. The objectives of the present work are to (i) study the effect of the machining parameters on the BUL formation and (ii) examine the validity of the optimal solution (TOPSIS) by qualitative assessment. The validity check for the optimal solution by qualitative assessment is a new approach.

Materials and Methods

The chemical composition of EN 36C work material was 0.159%C, 0.386%Mn, 0.182%Si, 0.820%Cr, 0.131%Mo, 3.100%Ni, 0.0182%Al, 0.0199%S, and 0.0164%P. The cylindrical work material was received for the machining. The diameter of the work material was 110 mm, and the length of the work material was 400 mm. The dry turning was done by using the Tungaloy SNMG 120404 (TM-T 9125) coated carbide insert (rake angle = 6° and main cutting-edge angle = 75°). The Taguchi's L_{27} orthogonal array design plan was selected for the experimentation. The process parameters, the levels, and the codes are shown (Table 1).

The Taguchi model is feasible because it helps to analyse the machining responses in an ordered manner. The feed and DOC are arranged orderly for low, moderate, and high speeds. The experimental numbers and the input parameter codes are considered according to the sequence as shown in table 2. The thickness (mm) of the chip was determined. The chips were viewed in the SEM. The chip reduction coefficients were obtained by using equation 1.

$$CRC = \frac{T2}{T1} \quad (1)$$

Where, *T1* is the un-deformed chip thickness and *T2* is the chip thickness. The chip surfaces were viewed by using a scanning electron microscope. The BUL formation was identified by the EDX. The universal tensile testing machine was used for the tensile test of the work material. The tensile test specimen was made according to standard ASTM E8 (test conditions: strain rate: 1 mm/mm, gauge length: 12.566 mm, and area: 26.431 mm^2). The power law equation (equation 2) was formed by conducting the tensile test for the specimen.

$$S = k \in^n \quad (2)$$

Where, S = true stress, k = strength coefficient, n = strain hardening exponent, and ϵ = true strain. The VMS (V) [15] can be given by equation 3.

Table 1: Machining parameters and codes.

Parameters/Codes	v, (m/min)	f, (mm/rev)	DOC, (mm)
Low: (1)	36	0.49	0.67
Moderate: (2)	60	0.63	1.0
High: (3)	100	0.86	1.5

Table 2: Experiment numbers and input parameter codes (Lowest: -1, Moderate: 0, and Highest: 1).

Expt. No. (codes)	Expt. No. (codes)	Expt. No. (codes)
1(-1, -1, -1)	10(0, -1, -1)	19(1, -1, -1)
2(-1, -1, 0)	11(0, -1, 0)	20(1, -1, 0)
3(-1, -1, 1)	12(0, -1 ,1)	21(1, -1, 1)
4(-1, 0, -1)	13(0, 0, -1)	22(1, 0, -1)
5(-1, 0 ,0)	14(0, 0, 0)	23(1, 0, 0)
6(-1, 0, 1)	15(0, 0, 1)	24(1, 0, 1)
7(-1, 1, -1)	16(0, 1, -1)	25(1, 1, -1)
8(-1, 1, 0)	17(0 ,1, 0)	26(1, 1, 0)
9(-1, 1 ,1)	18(0, 1, 1)	27(1, 1, 1)

$$V = 1.74 * k * (\ln \zeta)^n \quad (3)$$

Where, ζ = CRC. The CRC and the VMS were the objectives for the analysis (TOPSIS). Thereafter, the closeness coefficients were obtained by using the TOPSIS method. All steps of the TOPSIS method [12-14] were followed to find the optimal condition.

Results and Discussion

The stress-strain properties of the material were obtained (peak stress: 844.577 MPa, peak load: 22.323 kN, 0.2% offset yield stress: 580.507 MPa, yield load: 15.344 kN, modulus: 204.011 GPa, and elongation at break: 22.085%). Using the engineering stress-strain graph, a true stress-true strain graph was obtained. Three points between yield and ultimate strength were considered. Subsequently, true stress and true strain for the three points were plotted on log-log paper. From the graph, the true stress corresponding to a true strain of 1 will be the value of "K". The slope of the straight line in the graph is the value of "n". The tensile test specimen was made according to standard ASTM E8. The coefficient and exponent n of equation 4 were found.

$$S = 1495 \in^{0.178} \quad (4)$$

The experiment number, CRC, and the VMS (MPa) are sequentially shown in table 3. The normalized CRC, VMS, and the weighted normalized values were obtained by using the usual equations (Table 4 and table 5). The obtained closeness coefficients (CC) (after separation measures) and ranks are shown in Table 6. The closeness coefficients are also shown in figure 1a. The highest closeness coefficient was obtained for experiment number 22. So, the optimal process parameters were identified for experiment number = 22 (Rank 1), i.e., at (10 -1) [speed: high (v = 1), feed: moderate (f = 0), DOC: low (DOC = -1)]. The acceptable result is for v = 1(region). The possibility of BUL formation is higher for the v = 1 (region).

Table 3: CRC and VMS.

Expt. no./CRC/VMS (MPa)	Expt. no./CRC/ VMS (MPa)	Expt. no./CRC/VMS (MPa)
1/1.3/2067.7	10/1.8/2359.2	19/1.0/1468.4
2/1.2/1829.8	11/1.9/2412.4	20/1.1/1746.9
3/1.5/2191.2	12/1.4/2183.3	21/1.1/1797.8
4/1.2/1907.8	13/1.4/2134.6	22/1.0/1032.2
5/1.1/1605.2	14/1.7/2326.7	23/1.1/1639.8
6/1.0/1447.5	15/1.0/1351.8	24/1.3/2013.0
7/1.5/2191.5	16/1.4/2167.6	25/1.3/2080.2
8/1.0/1099.9	17/1.2/1963.8	26/1.1/1552.2
9/1.6/2268.7	18/1.3/2078.2	27/1.3/2064.4

Table 4: Normalized values.

Expt. no./CRC/VMS (MPa)	Expt. no./CRC/VMS (MPa)	Expt. no./CRC/VMS (MPa)
1/0.1931/0.2068	10/0.2604/0.2360	19/0.1522/0.1469
2/0.1682/0.1830	11/0.2809/0.2413	20/0.1624/0.1747
3/0.2136/0.2192	12/0.2121/0.2184	21/0.1653/0.1798
4/0.1741/0.1908	13/0.2034/0.2135	22/0.1478/0.1032
5/0.1565/0.1605	14/0.2502/0.2327	23/0.1580/0.1640
6/0.1522/0.1448	15/0.1507/0.1352	24/0.1858/0.2013
7/0.2136/0.2192	16/0.2092/0.2168	25/0.1946/0.2081
8/0.1478/0.1100	17/0.1800/0.1964	26/0.1551/0.552
9/0.2326/0.2269	18/0.1946/0.2079	27/0.1917/0.2065

Table 5: Weighted normalized values.

Expt. no./CRC VMS	Expt. no./CRC VMS	Expt. no./CRC VMS
1/0.0966/0.1034	10/0.1302/0.1180	19/0.0761/0.0734
2/0.0841/0.0915	11/0.1405/0.1206	20/0.0812/0.0874
3/0.1068/0.1096	12/0.1061/0.1092	21/0.0827/0.0899
4/0.0871/0.0954	13/0.1017/0.1067	22/0.0739/0.0516
5/0.0783/0.0803	14/0.1251/0.1164	23/0.0790/0.0820
6/0.0761/0.0724	15/0.0753/0.0676	24/0.0929/0.1007
7/0.1068/0.1096	16/0.1046/0.1084	25/0.0973/0.1040
8/0.0739/0.0550	17/0.0900/0.0982	26/0.0775/0.0776
9/0.1163/0.1135	18/0.0973/0.1039	27/0.0958/0.1032

Table 6: Closeness coefficients after separation measures.

Expt. no./CC	Rank	Expt. no./CC	Rank	Expt. no./CC	Rank
1/0.4548	16	10/0.1084	26	19/0.7845	5
2/0.6063	11	11/0	27	20/0.6507	9
3/0.3470	21	12/0.3546	21	21/0.6250	10
4/0.5636	12	13/0.4001	19	22/1	1
5/0.7189	7	14/0.1619	25	23/0.7020	8
6/0.7939	4	15/0.8395	3	24/0.4950	14
7/0.3469	23	16/0.3698	20	25/0.4462	18
8/0.9651	2	17/0.5284	13	26/0.7437	6
9/0.2514	23	18/0.4468	17	27/0.4606	15

The BUL prone domain is shown (Figure 1a). The interaction amongst the parameters is identified (solid green line, solid red line, and dashed black line) (Figure 1b). The influence of the feed on the VMS for the specific machining conditions (v = 1 and d = -1) is noted (solid yellow line, figure 1b). Such an influence causes the optimum VMS for f = 0. The TOPSIS method also identified the optimum solution for (1 0 -1), i.e., for the highest speed, moderate feed, and lowest DOC. The influence of a parameter on the machining process is for the concerned parameters only. The morphologies of the chip types at the different experimental speeds are shown in figure 2. The types of chips at the low speeds (experiment numbers 1 to 9) are broken types. The average chip breakability index was observed to be very high. This is attributed to the material strain hardening for the lower speeds. The average chip breakability index was moderately higher for medium speeds (experiment numbers 10 to 18). This is due to the strain hardening effect and partial thermal softening effect. The average chip break-

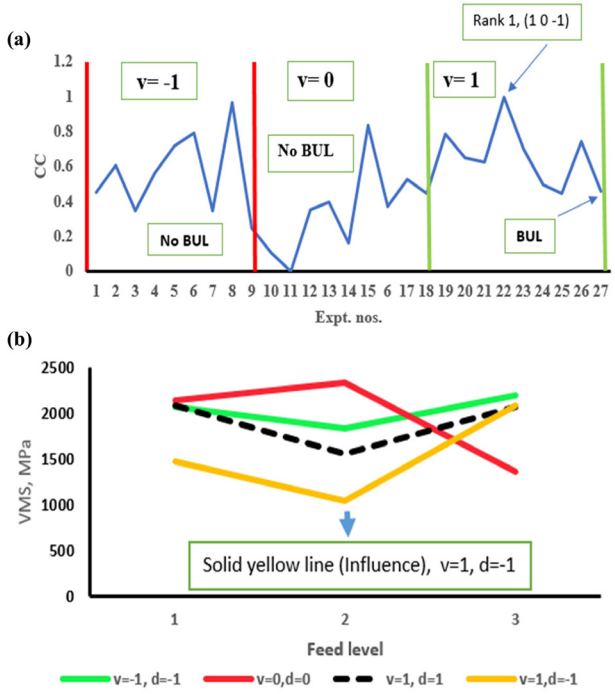

Figure 1: (a) Closeness coefficients with respect to experiment numbers. **(b)** The effect of interaction amongst parameters, (v = -1, DOC = -1, Solid green line; V = 0, DOC = 0, Solid red line; v = 1, DOC = 1, Dashed black line) and influence of the feed on the VMS (Solid yellow line).

Figure 2: Chip types at different speeds and experiments.

ability index for the high speeds (experiment numbers 19 to 27) has been observed to be very low. This is attributed to the predominating thermal softening effect (Figure 2). At low speed, the serrations form during the process of chip formation. This is due to the chip formation at non-uniform strains. The material side flow, the material sticking action, etc., were not observed at the undersurface of the chip. The inclusions were not observed at the surface (underside) of the chip (Figure 3a). The cracks are seen at the top surface as well as at the side surfaces (Figure 3b and 3c) of the chip. This shows that chip formation was mainly through the strain hardening mechanism. This is in agreement with the previous findings on chip morphologies. The VMS was relatively higher due to the strain hardening for this machining condition. The fracturing of the chip occurred through the brittle mode, as seen in the SEM image (Figure 3d). Thus, it is indicated that the chip formation occurred in an unfavorable mode. At moderate speed, the inclusions were found at the chip surface (under) (Figure 4a). The side flow of the material was also observed (Figure 4b). The chip formation was done through the successive shear sliding mechanism. The shear flow lines in the chips are seen (Figure 4c). This indicated that the chip formation was mainly due to the ductile transition of the material. This finding is further supported by the higher values of the CRC and the VMS in this machining condition (avg. CC lower). At high speed, the inclusions were not seen at the chip surface (under). The material side flow or the material sticking action or crack were not found at the chip surface (under) (Figure 5a). The serrations were also not observed. The chips formed at the uniform strains. The continuous chips form through the shear sliding mechanism. Thermal softening dominates to cause continuous chip formation (Figure 5b). The deformed recrystallized grains were noted (Figure 5c). The higher temperature causes the recrystallization in the chip during the process of chip formation. The recrystallized grains are deformed successively (Figure 5d). The thermal softening effect dominates the strain hardening effect. The fracture occurred in the finer grain chip material (Figure 5e). The favorable chip formation mode is revealed. The higher speed machining is favorable from the point of view of the chip formation mode. This is in agreement with the optimal result of the TOPSIS method. The built-up layer on the tool rake face is clearly seen in the electron image (Figure 5f). This is attributed to the presence of the inclusions. The EDX spectrum at the rake face also indicated the presence of inclusions (Figure 5g). The inclusions take part to form the BUL on the tool rake face. The weight percentages of elements in the BUL were found (C 69.29, O 15.38, Na 2.27, Mg 0.12, Al 1.13, Si 0.16, P 0.19, S 0.84, Cl 3.93, K 2.45, Ca 1.03, Ti 2.78, and Fe 0.45). Tool wear is inhibited due to the BUL.

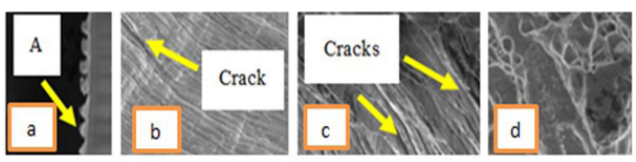

Figure 3: The SEM images of chips at low speed, feed, and DOC. **(a)** Under surface, A: serrations, X250; **(b)** Top surface, X1000; **(c)** Side surface, X2000; **(d)** Fracture surface, X3000 (v = 36 m/min, f = 0.49 mm/rev, and DOC = 0.67 mm).

Figure 4: The SEM images of the chip at moderate speed, feed, and DOC. **(a)** Under surface, X250; **(b)** Side surface, X500; **(c)** Side surface, X2000 (v = 60 m/min, f = 0.63 mm/rev, and DOC = 1 mm).

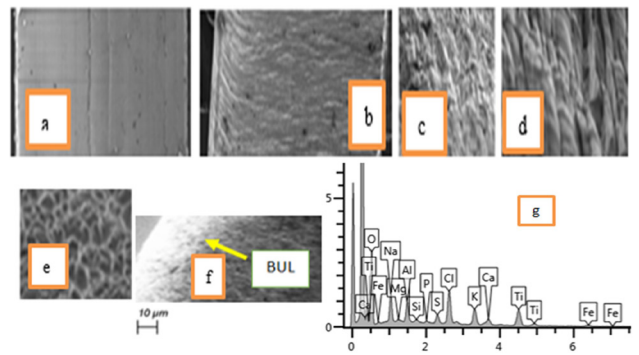

Figure 5: The SEM images of chip at high speed, feed, and DOC. **(a)** Under surface, X150; **(b)** Top surface, X150; **(c)** Side surface, X500; **(d)** Side surface, X3000; **(e)** Fracture surface, X5000 (v = 100 m/min, f = 0.86 mm/rev, and DOC = 1.5 mm); **(f)** BUL on the tool rake face; **(g)** The EDX spectrum (Y-axis: cps/eV).

The cutting forces and the extent of stress are also reduced due to the presence of the BUL. This occurs at the high-speed machining in the present study. Thus, it is observed that the machinability of the material is improved for high-speed machining. This is in agreement with the optimal solution as per the TOPSIS method. The BUL forms during the high-speed machining at the chip tool interface, and the chip slides over the BUL with minimal friction.

Conclusion

The Ni-Cr case hardened steel can be machined favorably due to the Ca and Mg de-oxidation. High speed machining for the alloy is preferable. The optimal machining parameters were identified for v = 100 m/min, feed = 0.63 mm/rev, and DOC = 0.67 mm. The strain hardening occurs, leading to the formation of the higher VMS for the low speed. The VMS and the CRC are less for high-speed machining because of the inclusion-based BUL formation. The optimality condition as per the TOPSIS method can be validated by the SEM examination and EDX analysis for the tool.

Acknowledgments

The tensile test and SEM examinations were done at IIT, Kanpur. The authors are grateful for that.

Conflict of Interest

There is no conflict of interest.

Credit Author Statement

Vishal Mishra: Writing - original draft preparation,

Writing - review and editing, Resources; Kalyan Chakraborty: Conceptualization, Methodology, Investigation, Formal analysis, Supervision. All the authors read and approved the manuscript.

References

1. Desaigues JE, Lescalier C, Bomont-Arzur A, Dudzinski D, Bomont O. 2016. Experimental study of built-up layer formation during machining of high strength free-cutting steel. *J Mater Process Technol* 236: 204-215. https://doi.org/10.1016/j.jmatprotec.2016.05.016
2. Mehmet BB. 2015. Investigating the effects of cutting parameters on the built-up-layer and built-up-edge formation during the machining of AISI 310 austenitic stainless steels. *Materiali Tehnologije* 49(5): 779-784. https://doi.org/10.17222/mit.2014.253
3. Larsson A, Ruppi S. 2001. Structure and composition of built-up layers on coated tools during turning of Ca-treated steel. *Mater Sci Eng A* 313(1-2): 160-169. https://doi.org/10.1016/S0921-5093(01)00964-9
4. Hoier P, Malakizadi A, Friebe S, Klement U, Krajnik P. 2019. Microstructural variations in 316L austenitic stainless steel and their influence on tool wear in machining. *Wear* 428: 315-327. https://doi.org/10.1016/j.wear.2019.02.024
5. Ånmark N, Björk T. 2016. Effects of the composition of Ca-rich inclusions on tool wear mechanisms during the hard-turning of steels for transmission components. *Wear* 368: 173-182. https://doi.org/10.1016/j.wear.2016.09.016
6. Maurya RK, Niranjan MS. 2022. Experimental analysis of mechanical behaviour and residual stresses of EN-36C alloy steel with and without tempering. *Proc Inst Mech Eng E J Process Mech Eng* 236(2), 214-224. https://doi.org/10.1177/09544089211038447
7. Ånmark N, Karasev A, Jönsson PG. 2015. The effect of different non-metallic inclusions on the machinability of steels. *Materials* 8(2): 751-783. https://doi.org/10.3390/ma8020751
8. Razzak MA. 2011. Heat treatment and effects of Cr and Ni in low alloy steel. *Bull Mater Sci* 34: 1439-1445. https://doi.org/10.1007/s12034-011-0340-9
9. Maisuradze MV, Björk T. 2022. Microstructure and mechanical properties of calcium treated 42CRMO4 steel with improved machinability. *Trans Indian Inst Met* 75(3): 681-690. https://doi.org/10.1007/s12666-021-02463-8
10. M'Saoubi R, Chandrasekaran H. 2011. Experimental study and modelling of tool temperature distribution in orthogonal cutting of AISI 316L and AISI 3115 steels. *Int J Adv Manuf Technol* 56: 865-877. https://doi.org/10.1007/s00170-011-3257-y
11. Shen P, Fu J. 2019. Morphology study on inclusion modifications using Mg–Ca treatment in resulfurized special steel. *Materials* 12(2): 197. https://doi.org/10.3390/ma12020197
12. Sahu AK, Sahu NK, Sahu AK, Rajput MS, Narang HK. 2019. T-SAW methodology for parametric evaluation of surface integrity aspects in AlMg3 (AA5754) alloy: comparison with T-TOPSIS methodology. *Measurement* 132: 309-323. https://doi.org/10.1016/j.measurement.2018.09.037
13. Balasubramaniyan S, Selvaraj T. 2017. Application of integrated Taguchi and TOPSIS method for optimization of process parameters for dimensional accuracy in turning of EN25 steel. *J Chin Inst Eng* 40(4): 267-274. https://doi.org/10.1080/02533839.2017.1308233
14. Sen B, Hussain SAI, Mia M, Mandal UK, Mondal SP. 2019. Selection of an ideal MQL-assisted milling condition: an NSGA-II-coupled TOPSIS approach for improving machinability of Inconel 690. *Int J Adv Manuf Technol* 103: 1811-1829. https://doi.org/10.1007/s00170-019-03620-6
15. Astakhov VP. 2006. Tribology of Metal Cutting. Elsevier